

1 Overview

The goal of the Daya Bay reactor antineutrino experiment is to determine the unknown neutrino mixing angle θ_{13} with a sensitivity of 0.01 or better in $\sin^2 2\theta_{13}$, an order of magnitude better than the current limit. This section provides an overview of neutrino oscillation phenomenology and the scientific requirements of the experiment.

1.1 Neutrino Oscillation Phenomenology

Compelling evidence for transformation of one neutrino flavor to another (neutrino oscillations) has been observed in solar [1–4], atmospheric [5], reactor [6] and accelerator [7,8] experiments, using a wide variety of detector technologies. The only consistent explanation for these results is that neutrinos have mass and that the mass eigenstates are not the same as the flavor eigenstates (neutrino mixing).

1.1.1 Neutrino Mixing

For three neutrino flavors, the mixing matrix, usually called the Maki-Nakagawa-Sakata-Pontecorvo [9] mixing matrix, is defined to transform the mass eigenstates (ν_1, ν_2, ν_3) to the flavor eigenstates (ν_e, ν_μ, ν_τ) and can be parameterized as

$$\begin{aligned}
 U_{\text{MNSP}} &= \begin{pmatrix} 1 & 0 & 0 \\ 0 & C_{23} & S_{23} \\ 0 & -S_{23} & C_{23} \end{pmatrix} \begin{pmatrix} C_{13} & 0 & \hat{S}_{13}^* \\ 0 & 1 & 0 \\ -\hat{S}_{13} & 0 & C_{13} \end{pmatrix} \begin{pmatrix} C_{12} & S_{12} & 0 \\ -S_{12} & C_{12} & 0 \\ 0 & 0 & 1 \end{pmatrix} \begin{pmatrix} e^{i\phi_1} & & \\ & e^{i\phi_2} & \\ & & 1 \end{pmatrix} \\
 &= \begin{pmatrix} C_{12}C_{13} & C_{13}S_{12} & \hat{S}_{13}^* \\ -S_{12}C_{23} - C_{12}\hat{S}_{13}S_{23} & C_{12}C_{23} - S_{12}\hat{S}_{13}S_{23} & C_{13}S_{23} \\ S_{12}S_{23} - C_{12}\hat{S}_{13}C_{23} & -C_{12}S_{23} - S_{12}\hat{S}_{13}C_{23} & C_{13}C_{23} \end{pmatrix} \begin{pmatrix} e^{i\phi_1} & & \\ & e^{i\phi_2} & \\ & & 1 \end{pmatrix} \quad (1)
 \end{aligned}$$

where $C_{jk} = \cos \theta_{jk}$, $S_{jk} = \sin \theta_{jk}$, $\hat{S}_{13} = e^{i\delta_{CP}} \sin \theta_{13}$. The neutrino oscillation phenomenology is independent of the Majorana phases ϕ_1 and ϕ_2 .

Neutrino oscillations of three flavors are completely described by six parameters: three mixing angles $\theta_{12}, \theta_{13}, \theta_{23}$, two independent mass-squared differences, $\Delta m_{21}^2 \equiv m_2^2 - m_1^2$, $\Delta m_{32}^2 \equiv m_3^2 - m_2^2$, and one CP -violating phase δ_{CP} (note that $\Delta m_{31}^2 \equiv m_3^2 - m_1^2 = \Delta m_{32}^2 + \Delta m_{21}^2$).

1.1.2 Current Knowledge of Mixing Parameters

Results from solar, atmospheric, reactor, and accelerator neutrino experiments have been used to determine the mixing parameters separately and in global fits. The sixth parameter, the CP -violating phase δ_{CP} , is inaccessible to the present and near future oscillation experiments. We quote here the result of a recent global fit with 2σ (95% C.L.) ranges [10]:

$$\Delta m_{21}^2 = 7.92(1.00 \pm 0.09) \times 10^{-5} \text{ eV}^2 \quad \sin^2 \theta_{12} = 0.314(1.00_{-0.15}^{+0.18}) \quad (2)$$

$$|\Delta m_{32}^2| = 2.4(1.00_{-0.26}^{+0.21}) \times 10^{-3} \text{ eV}^2 \quad \sin^2 \theta_{23} = 0.44(1.00_{-0.22}^{+0.41}) \quad (3)$$

$$\sin^2 \theta_{13} = (0.9_{-0.9}^{+2.3}) \times 10^{-2} \quad (4)$$

Due to the absence of a signal, the global fits on θ_{13} result in upper bounds which vary significantly from one fit to another.

Another very recent global fit [11] with different inputs finds allowed ranges for the oscillation parameters that overlap significantly with the above results even at 1σ (68% C.L.). The latest MINOS neutrino oscillation results [8] significantly overlap those in the global fit [10]. All these signify the convergence to a set of accepted values of neutrino oscillation parameters Δm_{21}^2 , $|\Delta m_{32}^2|$, $\sin^2 \theta_{12}$, and $\sin^2 \theta_{23}$.

The central value of θ_{13} extracted from Eq. 4 is about 5° . This corresponds to a value of 0.036 for $\sin^2 2\theta_{13}$, which should be compared to the best upper limit of 0.17 at 90% C.L. for $\Delta m_{31}^2 = 2.5 \times 10^{-3}$

eV^2 obtained by Chooz (see Fig. 1.1). We can conclude that, unlike θ_{12} and θ_{23} , the mixing angle θ_{13} is relatively small. The three parameters that are not determined by present data are θ_{13} , the sign of Δm_{32}^2

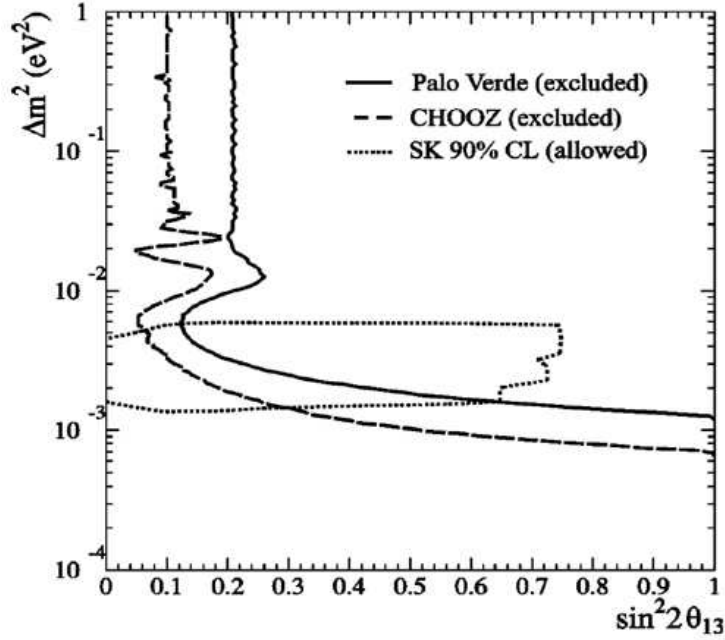


Fig. 1.1. Exclusion contours determined by Chooz, Palo Verde along with the allowed region obtained by Kamiokande. [12]

(which fixes the hierarchy of neutrino masses), and the Dirac CP -violating phase δ_{CP} .

1.1.3 Significance of the Mixing Angle θ_{13}

As one of the six neutrino mass parameters measurable in neutrino oscillations, θ_{13} is important in its own right and for further studies of neutrino oscillations. We need to know the value of θ_{13} to sufficient precision to design experiments to measure δ_{CP} . The matter effect, which can be used to determine the mass hierarchy, also depends on the size of θ_{13} . If $\theta_{13} > 0.01$, then the design of future experiments searching for CP violation is relatively straightforward [13]. However, for smaller θ_{13} new experimental techniques and accelerator technologies are likely required to carry out the measurements. In addition, θ_{13} is important in theoretical model building of the neutrino mass matrix, which can serve as a guide to the theoretical understanding of physics beyond the standard model. Based on these many considerations it is highly desirable to significantly improve our knowledge of θ_{13} in the near future. The February 28, 2006 report of the Neutrino Scientific Assessment Group (NuSAG) [14], which advises the DOE Offices of Nuclear Physics and High Energy Physics and the National Science Foundation, and the APS multi-divisional study's report on neutrino physics, *the Neutrino Matrix* [15], both recommend with high priority a reactor antineutrino experiment to measure $\sin^2 2\theta_{13}$ at the level of 0.01.

1.2 Determining θ_{13} with Nuclear Reactors

Reactor-based antineutrino experiments have the potential of uniquely determining θ_{13} at low cost and in a timely fashion. In this section we summarize the important features of nuclear reactors which are crucial to reactor-based antineutrino experiments.

1.2.1 Energy Spectrum and Flux of Reactor Antineutrinos

Many reactor antineutrino experiments to date have been carried out at pressurized water reactors (PWRs). Such a nuclear power plant derives its power from the fission of uranium and plutonium isotopes (mostly ^{235}U and ^{239}Pu) which are embedded in the fuel rods in the reactor core. The fission produces daughters, many of which beta decay because they are neutron-rich. Each fission on average releases approximately 200 MeV of energy and six antineutrinos. A typical reactor with 3 GW of thermal power (3 GW_{th}) emits 6×10^{20} antineutrinos per second with antineutrino energies up to 8 MeV. The majority of the antineutrinos have very low energies; about 75% are below 1.8 MeV, the threshold of the inverse beta-decay reaction (IBD) that will be discussed in Section 1.2.2.

The antineutrino flux and energy spectrum of a PWR depend on several factors: the total thermal power of the reactor, the fraction of each fissile isotopes in the fuel, the fission rate of each fissile isotope, and the energy spectrum of antineutrinos of the individual fissile isotopes.

The antineutrino yield is directly proportional to the thermal power that is determined by measuring the temperature, pressure and the flow rate of the cooling water. The reactor thermal power is measured continuously by the power plant with a typical precision of about 1%.

Fissile materials in a reactor are continuously consumed while new fissile isotopes are produced from other fissionable isotopes in the fuel (mainly ^{238}U) by fast neutrons. Since the antineutrino energy spectra are slightly different for the four main isotopes, ^{235}U , ^{238}U , ^{239}Pu , and ^{241}Pu , the knowledge on the fission composition and its evolution over time are therefore critical to the determination of the antineutrino flux and energy spectrum. From the average thermal power and the effective energy released per fission [16], the average number of fissions per second of each isotope can be calculated as a function of time. Figure 1.2 shows the results of a computer simulation of the Palo Verde reactor cores [17].

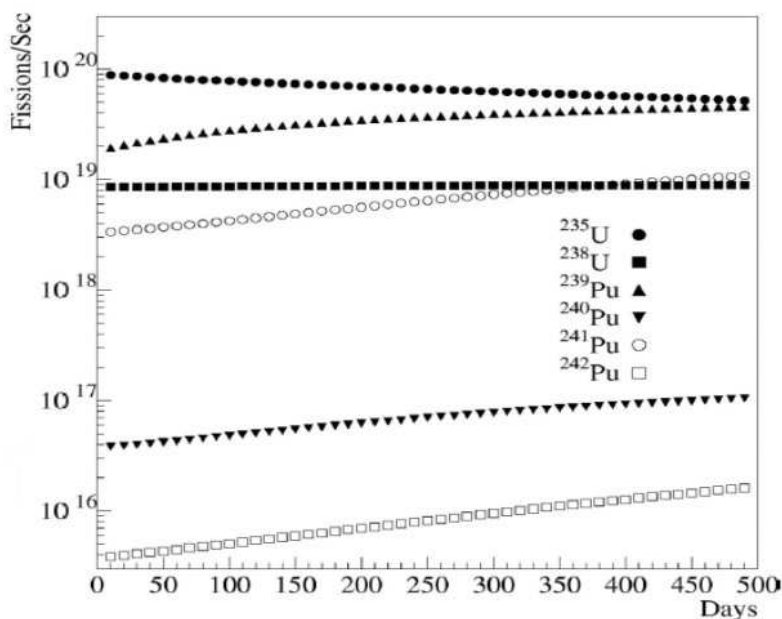


Fig. 1.2. Fission rate of reactor isotopes as a function of time from a Monte Carlo simulation [17].

It is common for a nuclear power plant to replace some of the fuel rods in the core periodically as the fuel is used up. Typically, a core will have 1/3 of its fuel changed every 12 to 18 months. At the beginning of each refueling cycle, 69% of the fissions are from ^{235}U , 21% from ^{239}Pu , 7% from ^{238}U , and 3% from

^{241}Pu . During operation the fissile isotopes ^{239}Pu and ^{241}Pu are produced continuously from ^{238}U . Toward the end of the fuel cycle, the fission rates from ^{235}U and ^{239}Pu are about equal. The average (“standard”) fuel composition responsible for the fission processes is 58% of ^{235}U , 30% of ^{239}Pu , 7% of ^{238}U , and 5% ^{241}Pu [18].

In general, the composite antineutrino energy spectrum is a function of the time-dependent contributions of the various fissile isotopes to the fission process. The Bugey 3 experiment compared three different models of the antineutrino spectrum with its measurement [19]. Good agreement was observed with the model that made use of the $\bar{\nu}_e$ spectra derived from the β spectra [20] measured at the Institute Laue-Langevin (ILL). However, there is no data for ^{238}U ; only the theoretical prediction is used. The possible discrepancy between the predicted and the real spectra should not lead to significant errors since the contribution from ^{238}U is never higher than 8%. The overall normalization uncertainty of the ILL measured spectra is 1.9%. A global shape uncertainty is also introduced by the conversion procedure.

A widely used three-parameter parameterization of the antineutrino spectrum for the four main isotopes, as shown in Fig. 1.3, can be found in [21]. Per fission, ^{238}U produces the highest number of antineutrinos whereas ^{239}Pu generates the least. In addition, the spectra associated with ^{235}U and ^{241}Pu are almost identical.

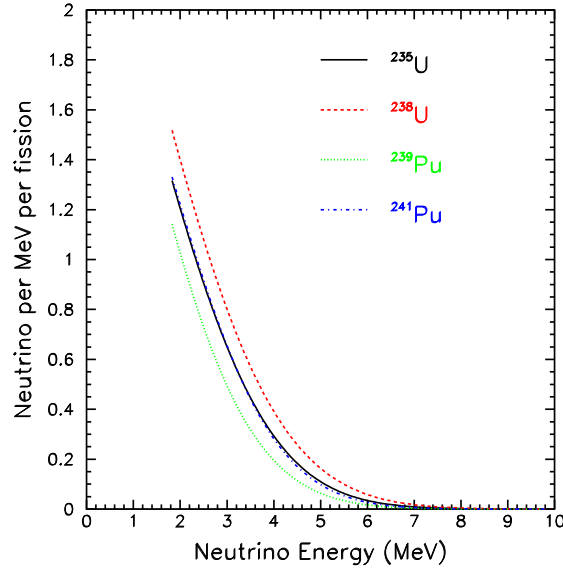


Fig. 1.3. Antineutrino energy spectrum for four isotopes following the parameterization of Vogel and Engel [21].

1.2.2 Inverse Beta-Decay Reaction

The reaction employed to detect the $\bar{\nu}_e$ from a reactor is the inverse beta-decay $\bar{\nu}_e + p \rightarrow e^+ + n$. The total cross section of this reaction, neglecting terms of order E_ν/M , where E_ν is the energy of the antineutrino and M is the nucleon mass, is

$$\sigma_{tot}^{(0)} = \sigma_0(f^2 + 3g^2)(E_e^{(0)}p_e^{(0)}/1\text{MeV}^2) \quad (5)$$

where $E_e^{(0)} = E_\nu - (M_n - M_p)$ is the positron energy when neutron recoil energy is neglected, and $p_e^{(0)}$ is the positron momentum. The weak coupling constants are $f = 1$ and $g = 1.26$, and σ_0 is related to the Fermi

coupling constant G_F , the Cabibbo angle θ_C , and an energy-independent inner radiative correction. The inverse beta-decay process has a threshold energy in the laboratory frame $E_\nu = [(m_n + m_e)^2 - m_p^2]/2m_p = 1.806$ MeV. The leading-order expression for the total cross section is

$$\sigma_{tot}^{(0)} = 0.0952 \times 10^{-42} \text{cm}^2 (E_e^{(0)} p_e^{(0)} / 1 \text{MeV}^2) \quad (6)$$

Vogel and Beacom [22] have recently extended the calculation of the total cross section and angular distribution to order $1/M$ for the inverse beta-decay reaction. Figure 1.4 shows the comparison of the total cross sections obtained in the leading order and the next-to-leading order calculations. Noticeable differences are

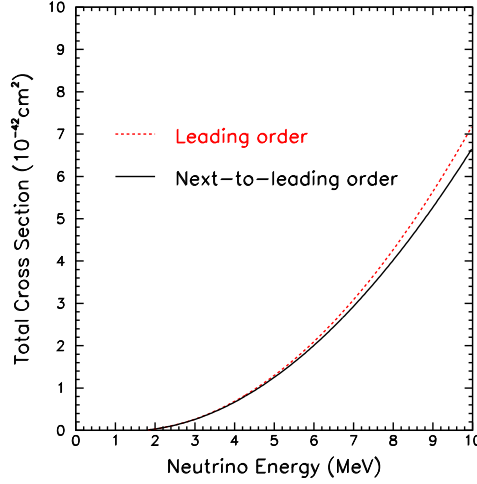


Fig. 1.4. Total cross section for inverse beta-decay calculated in leading order and next-to-leading order.

present for high antineutrino energies. We adopt the order $1/M$ formulae for describing the inverse beta-decay reaction. The calculated cross section can be related to the neutron lifetime, whose uncertainty is only 0.2%.

The expected recoil neutron energy spectrum, weighted by the antineutrino energy spectrum and the $\bar{\nu}_e + p \rightarrow e^+ + n$ cross section, is shown in Fig. 1.5. Due to the low antineutrino energy relative to the mass of the nucleon, the recoil neutron has low kinetic energy. While the positron angular distribution is slightly backward peaked in the laboratory frame, the angular distribution of the neutrons is strongly forward peaked, as shown in Fig. 1.6.

1.2.3 Observed Antineutrino Rate and Spectrum at Short Distance

The observed antineutrino spectrum is a product of the reactor antineutrino spectrum and the inverse beta-decay cross section. Figure 1.7 shows the differential antineutrino energy spectrum, the total cross section of the inverse beta-decay reaction, and the expected count rate as a function of the antineutrino energy. The differential energy distribution is the sum of the antineutrino spectra of all the radio-isotopes in the fuel. It is thus sensitive to the variation of thermal power and composition of the nuclear fuel.

By integrating over the energy of the antineutrino, the number of events can be determined. With one-ton* of LS, a typical rate is about 100 antineutrinos per day per GW_{th} at 100 m from the reactor.

*Throughout this document we will use the term ton to refer to a metric ton of 1000 kg.

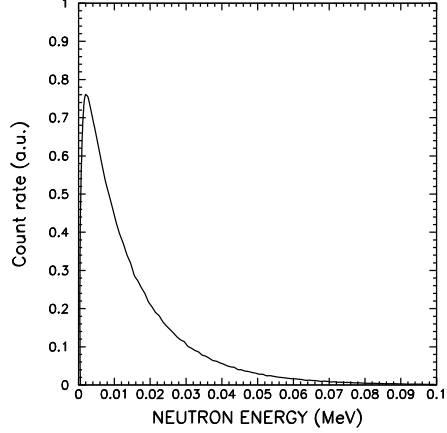


Fig. 1.5. Recoil neutron energy spectrum from inverse beta-decay weighted by the antineutrino energy spectrum.

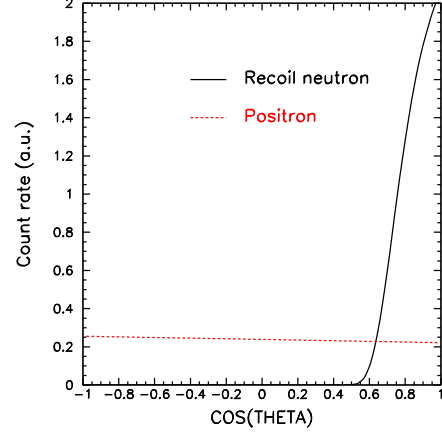


Fig. 1.6. Angular distributions of positrons and recoil neutrons from inverse beta-decay in the laboratory frame.

A small amount of Gd can be dissolved in the LS. After a moderation time of about ten μs , the neutron is captured by a Gd nucleus,[†] emitting several γ -ray photons with a total energy of about 8 MeV. This signal is called the delayed energy, E_d . The temporal correlation between the prompt energy (the positron signal) and the delayed energy constitutes a powerful tool for identifying the $\bar{\nu}_e$ and for suppressing backgrounds.

1.2.4 Reactor Antineutrino Disappearance Experiments

In a reactor-based antineutrino experiment the measured quantity is the survival probability for $\bar{\nu}_e \rightarrow \bar{\nu}_e$ at a baseline of the order of hundreds of meters to about a couple hundred kilometers with the $\bar{\nu}_e$ energy from about 1.8 MeV to 8 MeV. The matter effect is totally negligible and so the vacuum formula for the survival probability is valid. In the notation of Eq. 1, this probability has a simple expression

$$P_{\text{sur}} = 1 - C_{13}^4 \sin^2 2\theta_{12} \sin^2 \Delta_{21} - C_{12}^2 \sin^2 2\theta_{13} \sin^2 \Delta_{31} - S_{12}^2 \sin^2 2\theta_{13} \sin^2 \Delta_{32} \quad (7)$$

where

$$\begin{aligned} \Delta_{jk} &\equiv 1.267 \Delta m_{jk}^2 (\text{eV}^2) \times 10^3 \frac{L(\text{km})}{E(\text{MeV})} \\ \Delta m_{jk}^2 &\equiv m_j^2 - m_k^2 \end{aligned} \quad (8)$$

L is the baseline in km, E the antineutrino energy in MeV, and m_j the j -th antineutrino mass in eV. The $\nu_e \rightarrow \nu_e$ survival probability is given by Eq. 7 which is independent of the CP phase angle δ_{CP} and the mixing angle θ_{23} .

To obtain the value of θ_{13} , the depletion of $\bar{\nu}_e$ has to be extracted from the experimental $\bar{\nu}_e$ disappearance probability,

$$\begin{aligned} P_{\text{dis}} &\equiv 1 - P_{\text{sur}} \\ &= C_{13}^4 \sin^2 2\theta_{12} \sin^2 \Delta_{21} + C_{12}^2 \sin^2 2\theta_{13} \sin^2 \Delta_{31} + S_{12}^2 \sin^2 2\theta_{13} \sin^2 \Delta_{32} \end{aligned} \quad (9)$$

[†]The cross section of neutron capture by a proton is 0.3 b and 50,000 b on Gd for neutrons with kinetic energies on the order of tens of keV.

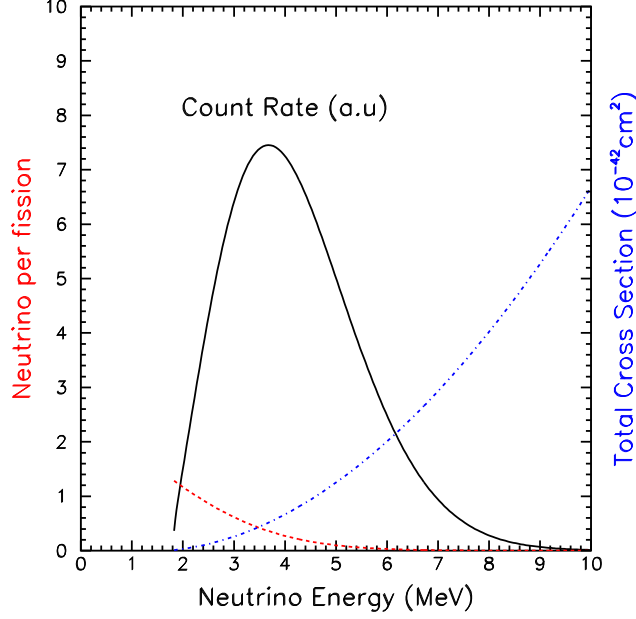


Fig. 1.7. Antineutrino energy spectrum (red dotted curve), total inverse beta-decay cross section (blue dotted-dash curve), and count rate (black solid curve) as a function of antineutrino energy.

Since θ_{13} is known to be less than 10° , we define the term that is insensitive to θ_{13} as

$$P_{12} = C_{13}^4 \sin^2 2\theta_{12} \sin^2 \Delta_{21} \approx \sin^2 2\theta_{12} \sin^2 \Delta_{21} \quad (10)$$

Then the part of the disappearance probability directly related to θ_{13} is given by

$$\begin{aligned} P_{13} &\equiv P_{\text{dis}} - P_{12} \\ &= +C_{12}^2 \sin^2 2\theta_{13} \sin^2 \Delta_{31} + S_{12}^2 \sin^2 2\theta_{13} \sin^2 \Delta_{32} \end{aligned} \quad (11)$$

The above discussion shows that in order to obtain θ_{13} we have to subtract the θ_{13} -insensitive contribution P_{12} from the experimental measurement of P_{dis} . To see their individual effect, we plot P_{13} in Fig. 1.8 together with P_{dis} and P_{12} as a function of the baseline from 100 m to 250 km. The antineutrino energy is integrated from 1.8 MeV to 8 MeV. We also take $\sin^2 2\theta_{13} = 0.10$, which will be used for illustration in most of the discussions in this section. The other parameters are taken to be

$$\theta_{12} = 34^\circ, \quad \Delta m_{21}^2 = 7.9 \times 10^{-5} \text{eV}^2, \quad \Delta m_{31}^2 = 2.5 \times 10^{-3} \text{eV}^2 \quad (12)$$

The behavior of the curves in Fig. 1.8 are quite clear from their definitions, Eqs. (9), (10), and (11). Below a couple kilometers P_{12} is very small, and P_{13} and P_{dis} track each other well. This suggests that the measurement can be best performed at the first oscillation maximum of $P_{13}(\text{max}) \simeq \sin^2 2\theta_{13}$. Beyond the first minimum P_{13} and P_{dis} deviate from each other more and more as L increases when P_{12} becomes dominant in P_{dis} .

When we determine $P_{13}(\text{max})$ from the difference $P_{\text{dis}} - P_{12}$, the uncertainties on θ_{12} and Δm_{21}^2 will propagate to P_{13} . It is easy to check that, given the best fit values in Eq. 2, when $\sin^2 2\theta_{13}$ varies from 0.01 to

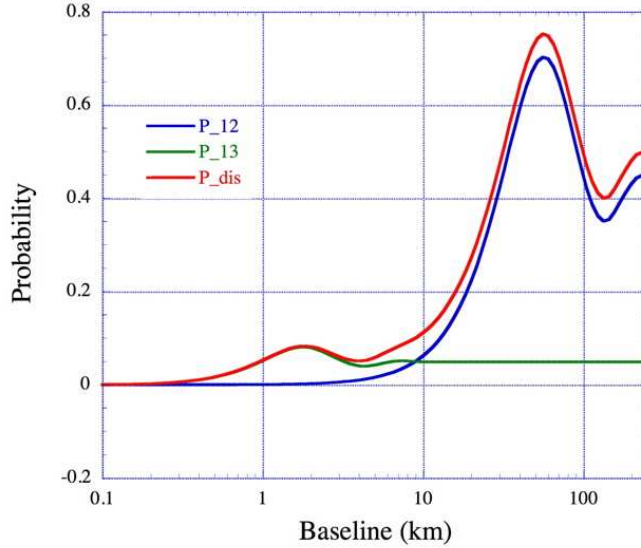


Fig. 1.8. Reactor antineutrino disappearance probability as a function of distance from the source. The values of the mixing parameters are given in Eq. 12. P_{12} is the slowly rising blue curve. P_{13} is the green curve that has a maximum near 2 km. The total disappearance probability P_{dis} is the red curve.

0.10 the relative size of P_{12} compared to P_{13} is about 25% to 2.6% at the first oscillation maximum. Yet the contribution of the uncertainty of P_{12} to the uncertainty in determining $\sin^2 2\theta_{13}$ is always less than 0.005.

In Fig. 1.9, P_{dis} integrated over E from 1.8 to 8 MeV is shown as a function of the baseline L for three values of Δm_{32}^2 that cover the allowed range of Δm_{32}^2 at 95% C.L. as given in Eq. 3. The curves show the location of the oscillation maximum is sensitive to Δm_{32}^2 . For $\Delta m_{32}^2 = (1.8, 2.4, 2.9) \times 10^{-3} \text{ eV}^2$, the oscillation maximum occurs at a baseline of 2.5 km, 1.9 km, and 1.5 km, respectively. From this simple study, placing the detector between 1.5 km and 2.5 km from the reactor looks to be a good choice.

We conclude from this phenomenological investigation that the choice of L be made so that it can cover as large a range of Δm_{31}^2 as possible. A baseline near 2 km is particularly attractive since it is least sensitive to the value of Δm_{31}^2 .

1.2.5 Precision Measurement of θ_{13}

The value of $\sin^2 2\theta_{13}$ can be determined by comparing the observed antineutrino rate and energy spectrum with predictions assuming no oscillations. The number of detected antineutrinos N_{det} is given by

$$N_{\text{det}} = \frac{N_p}{4\pi L^2} \int \epsilon \sigma P_{\text{sur}} S dE \quad (13)$$

where N_p is the number of free protons in the target, L is the distance of the detector from the reactor, ϵ is the efficiency of detecting an antineutrino, σ is the total cross section of the inverse beta-decay process, P_{sur} is the survival probability given in Eq. 7, and S is the differential energy distribution of the antineutrino at the reactor shown in Fig. 1.7.

With only one detector at a fixed baseline from a reactor, according to Eq. 13, we must determine the

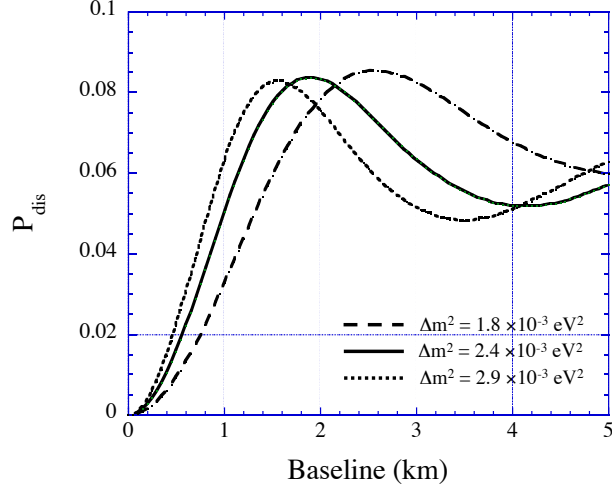


Fig. 1.9. Reactor antineutrino disappearance probability due to the mixing angle θ_{13} as a function of the baseline L over the allowed 2σ range in Δm_{32}^2 .

absolute antineutrino flux from the reactor, the absolute cross section of the inverse beta-decay reaction, and the efficiencies of the detector and event-selection requirements in order to measure $\sin^2 2\theta_{13}$. The prospect for determining $\sin^2 2\theta_{13}$ precisely with a single detector is not promising. It is a challenge to reduce the systematic uncertainties of such an absolute measurement to sub-percent level, especially for reactor-related uncertainties.

Mikaelyan and Sinev pointed out that the systematic uncertainties can be greatly suppressed or totally eliminated when two detectors positioned at two different baselines are utilized [23]. The near detector close to the reactor core is used to establish the flux and energy spectrum of the antineutrinos. This relaxes the requirement of knowing the details of the fission process and operational conditions of the reactor. In this approach, the value of $\sin^2 2\theta_{13}$ can be measured by comparing the antineutrino flux and energy distribution observed with the far detector to those of the near detector after scaling with distance squared. According to Eq. 13, the ratio of the number of antineutrino events with energy between E and $E + dE$ detected at distance L_f (far detector) to that at a baseline L_n (near detector) is given by

$$\frac{N_f}{N_n} = \left(\frac{N_{p,f}}{N_{p,n}} \right) \left(\frac{L_n}{L_f} \right)^2 \left(\frac{\epsilon_f}{\epsilon_n} \right) \left[\frac{P_{\text{sur}}(E, L_f)}{P_{\text{sur}}(E, L_n)} \right] \quad (14)$$

By placing the near detector close to the core such that there is no significant oscillating effect and the contribution of θ_{12} is negligible, $\sin^2 2\theta_{13}$ is approximately given by

$$\sin^2 2\theta_{13} \approx \frac{1}{A(E, L_f)} \left[1 - \epsilon_r \left(\frac{N_f}{N_n} \right) \left(\frac{L_f}{L_n} \right)^2 \right] \quad (15)$$

where $A(E, L_f) = \sin^2 \Delta_{31}$ with Δ_{31} defined in Eq. 8 is the analyzing power and ϵ_r is the relative efficiency of the near and far detectors. The relative detector efficiency can be determined more precisely than the absolute efficiency. Indeed, from this simplified picture, it is clear that the two-detector scheme is an excellent

approach for precisely determining the value of $\sin^2 2\theta_{13}$. In practice, we need to extend this idea to handle more complicated arrangements involving multiple reactors and multiple detectors as in the case of the Daya Bay experiment.

1.2.6 Requirements for a Precision Measurement of θ_{13} with Reactors

As discussed in Section 1.2.4, probing $\sin^2 2\theta_{13}$ with a sensitivity of 0.01 will be a significant advance in neutrino physics. In order to meet this goal, it is important to reduce the statistical and systematic uncertainties as well as to suppress backgrounds. A sensitivity of 0.01 (90% C.L.) implies the standard deviation of the measurement is about 0.0061 for a one-parameter fit (namely, $\sin^2 2\theta_{13}$).

- **High Statistics** The statistical uncertainty of this measurement is dominated by the total number of antineutrino events detected with the far detector that depends on the thermal power of the nuclear power plant, the target mass, and the amount of running time.
- **Optimization of baselines** In the generic design with two detectors, the near detector should be positioned as close to the reactor as possible so that the flux and the energy spectrum of the antineutrinos are not significantly affected by oscillations. The far detector should be placed near the first oscillation maximum, between 1.5 km and 2 km, so as to maximize the disappearance probability (this also minimizes the dependence on Δm_{31}^2 as discussed in Section 1.2.4).
- **Reduction of systematic uncertainties** The two major sources of systematic uncertainties arise from variation of thermal power of the reactors and from slight variations in the performance and characteristics of the detectors. Since the uncertainty of this measurement is expected to be 0.0061, the total systematic uncertainty of the measurement must be controlled to better than this level. A significant fraction of the reactor-related systematic uncertainty can be removed by adopting a near-far arrangement of detectors as discussed in Section 1.2.5. In addition, since the value of $\sin^2 2\theta_{13}$ will be extracted by comparing the detected events in the near and far detectors, which is a *relative* measurement, the detector-related systematic uncertainty in this approach is greatly reduced. Furthermore, by ensuring the detectors are built to the same specifications, along with a comprehensive program of monitoring and calibration, it is expected that the total detector-related systematic uncertainty can be kept below the statistical uncertainty.
- **Background suppression** Since the signal rate is low, it is desirable to conduct the experiment underground to reduce cosmic-ray induced backgrounds from neutrons and the radioactive isotope ${}^9\text{Li}$. Gamma rays originating from natural radioactivity in construction materials and the surrounding rock can contribute to accidentals as the random coincidence of a γ ray interaction in the detector and a neutron capture can mimic the signal. Since Chooz [12] had an overburden of ~ 300 m.w.e. and achieved a background-to-signal ratio of approximately 0.09, the new generation of reactor-based θ_{13} experiments should have additional overburden and shielding enclosing the detectors to further suppress backgrounds.

1.2.7 Some Proposals for Precision Measurement of θ_{13} with Reactors

As of 2006, there are about 440 nuclear reactors producing electricity in the world. Approximately half of them are PWRs, the kind of reactor that all past reactor-based neutrino experiment have utilized. The majority of these PWRs being in France, Japan, and the United States. However, the majority of the most powerful PWR nuclear power plants reside in Japan [24][‡], South Korea [25], and France [26] with local physicists interested in mounting reactor θ_{13} experiments with sensitivities between 0.02 and 0.03.

[‡]KASKA in Japan is now mothballed.

Palo Verde, in the United States, is the twelfth most powerful reactor in the world. The plant operator has shown no interest in supporting another experiment. Furthermore, this site is flat within a radius of several km, which would necessitate construction of large, deep vertical shafts for deploying detectors.

A proposal to use the Diablo Canyon plant in California to perform the measurement [13] is now defunct. This is an attractive site, with a mountain range several hundred meters away from twin reactors with a total thermal power of $6.7 \text{ GW}_{\text{th}}$. The near site would be similar to Double Chooz requiring a slanted (or vertical) shaft to access the detector. However, environmental concerns and potential interference of the experiment's civil construction of the experiment with the plant's onsite waste storage terminated the project.

1.3 The Daya Bay Reactor Antineutrino Experiment

The objective of the Daya Bay experiment is to determine $\sin^2 2\theta_{13}$ with sensitivity of 0.01 or better. This experiment will be located at the Daya Bay nuclear power complex in southern China. Its location is shown in Fig. 1.10. The experimental site is about 55 km north-east from the Victoria Harbor in Hong Kong.

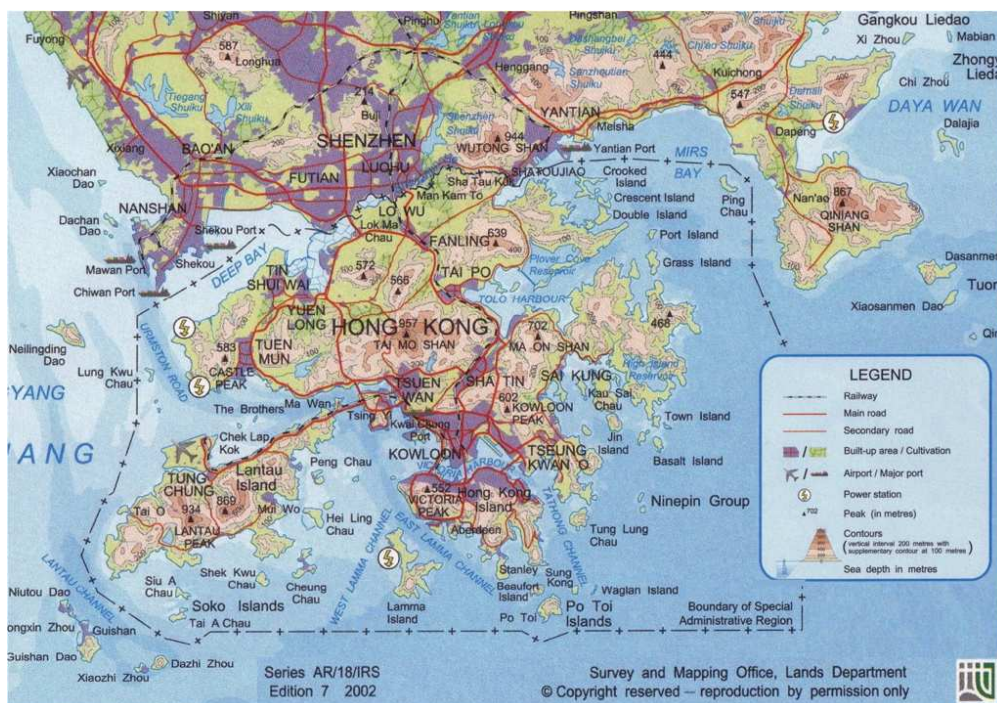


Fig. 1.10. Daya Bay and vicinity: The nuclear power complex is located 55 km from central Hong Kong on the bay “Daya Wan” at the upper right of the map.

Figure 1.11 is a photograph of the complex. The complex consists of three nuclear power plants (NPPs): the Daya Bay NPP, the Ling Ao NPP, and the Ling Ao II NPP. The Ling Ao II NPP is under construction and will be operational by 2010–2011. Each plant has two identical reactor cores. Each core generates $2.9 \text{ GW}_{\text{th}}$ during normal operation. The distance between the two cores in each NPP is about 88 m. The Ling Ao cores are about 1.1 km east of the Daya Bay cores, and about 400 m west of the Ling Ao II cores. There are mountain ranges to the north which provide sufficient overburden to suppress cosmogenic backgrounds in the underground experimental halls. Within 2 km of the site the elevation of the mountain varies generally from 185 m to 400 m.

The six cores can be roughly grouped into two clusters, the Daya Bay cluster of two cores and the Ling



Fig. 1.11. The Daya Bay nuclear power complex. The Daya Bay nuclear power plant is in the foreground. The Ling Ao nuclear power plant is in the background. The experimental halls will be underneath the hills to the left.

Ao cluster of four cores. We plan to deploy two identical sets of detectors near their respective cluster of cores, one primarily for the Daya Bay cores and the other for the Ling Ao—Ling Ao II cores, to monitor the antineutrino fluxes as precisely as possible. Another set of identical detectors, the far detectors, will be located north of the two near detector sets. Since the overburden of the experimental site increases with distance from the cores, the cosmogenic background decreases as the signal decreases, hence keeping the background-to-signal ratio roughly constant. This is beneficial to controlling systematic uncertainties.

1.3.1 Experimental layout

Taking the current value of $\Delta m_{31}^2 = 2.5 \times 10^{-3} \text{ eV}^2$ (see equation 12), the first maximum of the oscillation associated with θ_{13} occurs at $\sim 1800 \text{ m}$. Considerations based on statistics alone will result in a somewhat shorter baseline, especially when the statistical uncertainty is larger than or comparable to the systematic uncertainty. For the Daya Bay experiment, the overburden influences the optimization since it varies along the baseline. In addition, a shorter tunnel will decrease the civil construction cost.

Three major factors are involved in optimizing the locations of the near sites. The first one is overburden. The slope of the hills near the site is around 30 degrees. Hence, the overburden falls rapidly as the detector site is moved closer to the cores. The second concern is oscillation loss. The oscillation probability is appreciable even at the near sites. For example, for the near detectors placed approximately 500 m from the center of gravity of the cores, the integrated oscillation probability is $0.19 \times \sin^2 2\theta_{13}$ (computed with $\Delta m_{31}^2 = 2.5 \times 10^{-3} \text{ eV}^2$). The oscillation contribution of the other pair of cores, which is around 1100 m away, has been included. The third concern is the near-far cancellation of reactor uncertainties.

After careful study of many different experimental designs, the best configuration of the experiment is shown in Fig. 1.13 together with the tunnel layout. Based on this configuration, a global χ^2 fit (see Eq. ??) for the best sensitivity and baseline optimization was performed, taking into account backgrounds, mountain profile, detector systematics and residual reactor related uncertainties. The result is shown in Fig. 1.12.

Ideally each near detector site should be positioned equidistant from the cores that it monitors so that the uncorrelated reactor uncertainties are cancelled. However, taking overburden and statistics into account while optimizing the experimental sensitivity, the Daya Bay near detector site is best located 363 m from the center of the Daya Bay cores. The overburden at this location is 98 m (255 m.w.e.).[§] The Ling Ao near detector hall is optimized to be 481 m from the center of the Ling Ao cores, and 526 m from the center of

[§]The Daya Bay near detector site is about 40 m east of the perpendicular bisector of the Daya Bay two cores to gain more overburden.

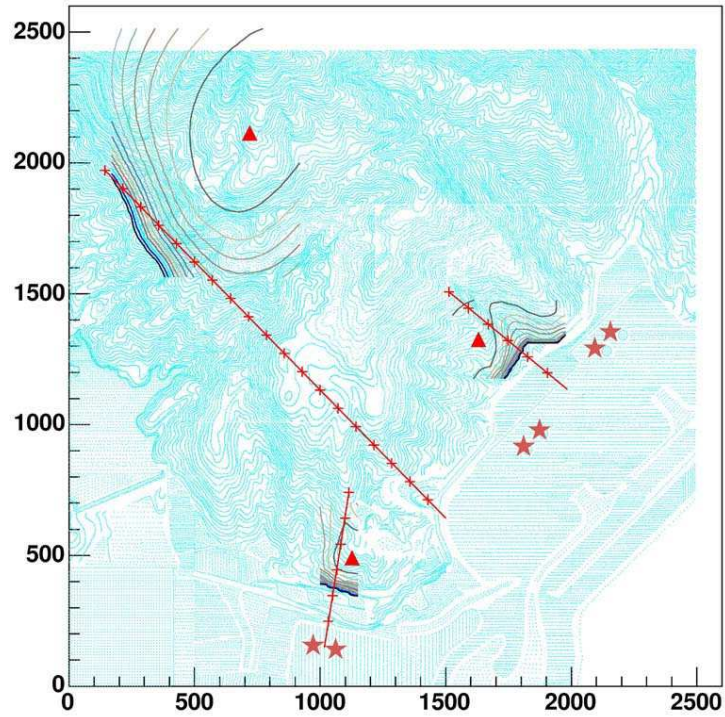


Fig. 1.12. Site optimization using the global χ^2 analysis. The optimal sites are labelled with red triangles. The stars show the reactors. The black contours show the sensitivity when one site's location is varied and the other two are fixed at optimal sites. The red lines with tick marks are the perpendicular bisectors of various combinations of reactors. The mountain contours are also shown on the plot (blue lines).

the Ling Ao II cores[¶] where the overburden is 112 m (291 m.w.e).

The far detector site is about 1.5 km north of the two near sites. Ideally the far site should be equidistant between the Daya Bay and Ling Ao—Ling Ao II cores; however, the overburden at that location would be only 200 m (520 m.w.e). At the optimized locations, the distances from the far detector to the midpoint of the Daya Bay cores and to the mid point of the Ling Ao—Ling Ao II cores are 1985 m and 1615 m, respectively. The overburden is about 350 m (910 m.w.e). A summary of the distances to each detector is provided in Table 1.1. The reactor-related systematic uncertainties cannot be cancelled completely, but can

	DYB	LA	Far
DYB cores	363	1347	1985
LA cores	857	481	1618
LA II cores	1307	526	1613

Table 1.1. Distances (in meters) from each detector site to the centroid of each pair of reactor cores.

be reduced to a negligible level. From the global fit, a residual reactor uncertainty of $<0.1\%$ is obtained.

There are three branches for the main tunnel extending from a junction near the mid hall to the near and far underground detector halls. There are also access and construction tunnels. The length of the access tunnel, from the portal to the Daya Bay near site, is 292 m. It has a grade of 9.6% [28], which allows the underground facilities to be located deeper with more overburden. The final layout of the underground facility is shown in Figure 1.13.

From the global baseline optimization, by comparing the antineutrino fluxes and energy spectra between the near and far detectors, we also conclude we need to collect 170,000 events with the far detector in order to establish the presence of neutrino oscillation due to θ_{13} , and to reach the designed sensitivity. Since the standard error will be 0.0061, Daya Bay would determine the central value of $\sin^2 2\theta_{13}$ derived from Eq. 4 with approximately a six-sigma significance. Table 1.2 is a summary of the scientific requirements for determining $\sin^2 2\theta_{13}$ with a sensitivity of 0.01 at the 90% confidence level.

Table 1.2. Summary of scientific requirements

Item	Requirement
Sensitivity in $\sin^2 2\theta_{13}$ (90% C.L.)	≤ 0.01
Standard error of $\sin^2 2\theta_{13}$	0.0061
Baseline of the far detector	≤ 2 km
Number of events at the far site	170,000
Background/signal	≤ 0.09

1.3.2 Detector Design

Besides collecting at least 170,000 antineutrino events at the far site, systematic uncertainties in the ratios of the near-to-far detector acceptance, antineutrino flux and background have to be controlled to a level almost an order of magnitude better than the previous experiments. Based on the recent single-detector reactor experiments such as Chooz, Palo Verde and KamLAND, there are three main sources of systematic

[¶]The Ling Ao near detector site is about 50 m west of the perpendicular bisector of the Ling Ao-Ling Ao II clusters to avoid installing it in a valley which is likely to be geologically weak, and to gain more overburden.

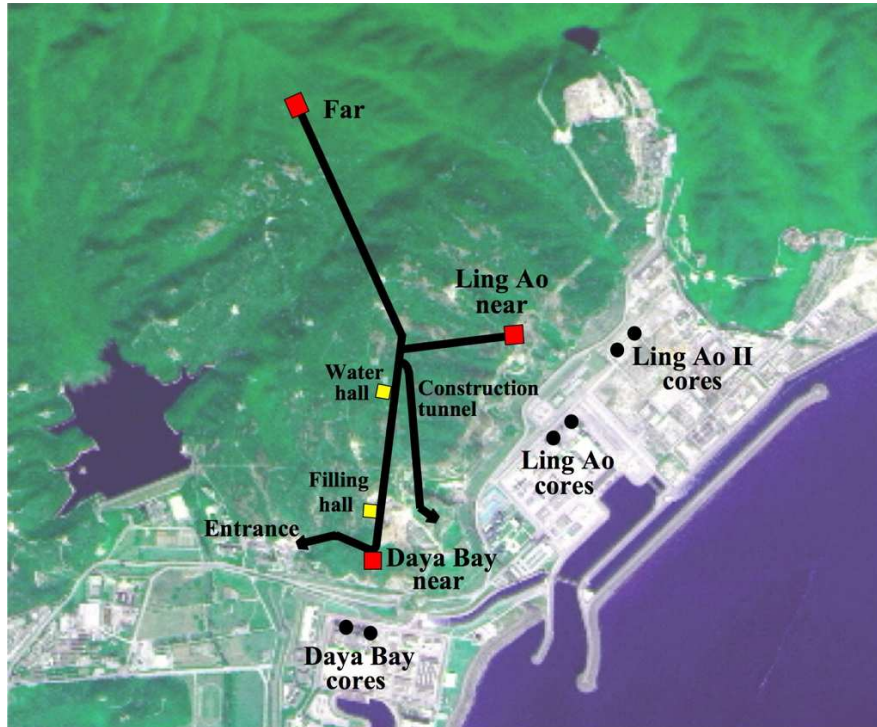


Fig. 1.13. Layout of the Daya Bay experiment.

uncertainty: reactor-related uncertainty of (2–3)%, background-related uncertainty of (1–3)%, and detector-related uncertainty of (1–3)%. Each source of uncertainty can be further classified into correlated and uncorrelated uncertainties. Hence a carefully designed experiment, including the detector mass, efficiency and background control, is required. The primary considerations driving the improved performance are listed below:

- **identical near and far detectors** As discussed in Section 1.2.6, identical antineutrino detectors will be deployed at the near and far sites to minimize the reactor- and detector-related systematic uncertainties. The event samples collected with the near detectors will be used to predict the characteristics of the events observed at the far detectors. Even with several cores at Daya Bay, reactor-related uncertainties can be controlled to a negligible level by carefully optimizing the near and far site locations.
- **multiple modules** multiple identical modules will be installed at the near and far sites to reduce detector-related uncorrelated uncertainties. The use of multiple modules in each site enables internal consistency checks (to the limit of statistics). In addition, multiple modules implies smaller detectors which are easier to move. Furthermore, small detectors intercept fewer cosmic-ray muons, resulting in less dead time, less cosmogenic background and hence smaller systematic uncertainty. Taking calibration and monitoring of the detectors, redundancy and cost into account, we have selected a design with two modules at each near site and four modules at the far site.
- **three-zone detector module** Each module is partitioned into three concentric zones. The innermost zone, filled with Gd-loaded liquid scintillator (Gd-LS), is the antineutrino target which is surrounded by a zone filled with unloaded LS called the γ -catcher. This middle zone is used to capture γ rays, from IBD events, that escape from the target. This arrangement can substantially reduce the systematic uncertainties related to the target volume and mass, positron energy threshold, and position cut. The

outermost zone, filled with transparent mineral oil that does not scintillate, shields against external γ rays entering the active LS volume.

- **sufficient overburden and shielding** The locations of all the underground detector halls are optimized to provide sufficient overburden to reduce the cosmogenic backgrounds to a level that can be measured with certainty. The antineutrino detector modules will be enclosed with sufficient passive shielding to attenuate natural radiation and energetic spallation neutrons from the surrounding rocks and materials used in the experiment.
- **multiple muon detectors** By tagging the incident muons, the associated cosmogenic background can be suppressed to a negligible level. This requires the muon detectors surrounding the antineutrino detectors to have a high efficiency that is known to high precision. Monte Carlo study shows that the efficiency of the muon detector should be $\geq 99.5\%$ (with $\sigma_\epsilon \leq 0.25\%$). The muon system is designed to have at least two detector systems in each direction. One system utilizes the water shield as a Cherenkov detector, and another employs muon tracking detectors with decent position resolution. Each muon detector can easily be constructed with an efficiency of (90–95)% such that the overall efficiency of the muon system will be better than 99.5%. In addition, the two muon detectors can be used to measure the efficiency of each other to a uncertainty of better than 0.25%.
- **movable detectors** The detector modules are movable, such that swapping of modules between the near and far sites can be employed to provide an even higher level of cancellation of the detector-related uncertainties (to the extent that they remain unchanged before and after swapping). The residual uncertainties, being secondary, are caused by the energy scale uncertainties not completely taken out by calibration, as well as other site-dependent uncertainties. The goal is to reduce the systematic uncertainties as much as possible by careful design and construction of detector modules such that swapping of detectors is not necessary. Further discussion of detector swapping will be given in Chapters ?? and ??.

With these improvements, the total detector-related systematic uncertainty is expected to be $\sim 0.2\%$ in the near-to-far ratio per detector site. As discussed above, the antineutrino detector employed at the near (far) site has two (four) modules while the muon detector consists of a cosmic-ray tracking device and active water shield. There are several possible configurations for the water shield and the muon tracking detector as discussed in Section ???. The baseline design of the far site is shown in Fig. 1.14.

The water shield in this case is a water pool, instrumented with photomultiplier tubes (PMTs) to serve as a Cherenkov detector. The outer region of the water pool is separated from the inner region by an optical barrier to provide two independent devices for detecting muons. Above the pool the muon tracking detector is made of light-weight resistive-plate chambers (RPCs). RPCs offer good performance and excellent position resolution at a low cost.

The antineutrino detector modules are submerged in the water pool, shielding them from ambient radiation and spallation neutrons. Alternate water shielding configurations are discussed in Section ??.

1.3.2.1 Antineutrino detector

As discussed in Sections 1.2.2 and 1.2.3 antineutrinos are detected via the inverse beta-decay reaction in Gd-LS. The prompt positron signal and delayed neutron-capture signal (8 MeV and capture time of 28 μs) are combined to define a neutrino event with timing and energy requirements on both signals. Both Chooz [29] and Palo Verde [30] used 0.1% Gd-loaded LS that yielded a capture time of 28 μs , about a factor of seven shorter than in the undoped LS. The large energy release and relatively short capture time provide good suppression of accidental backgrounds.

The specifications for the design of the Daya Bay antineutrino detector modules are given as follows:

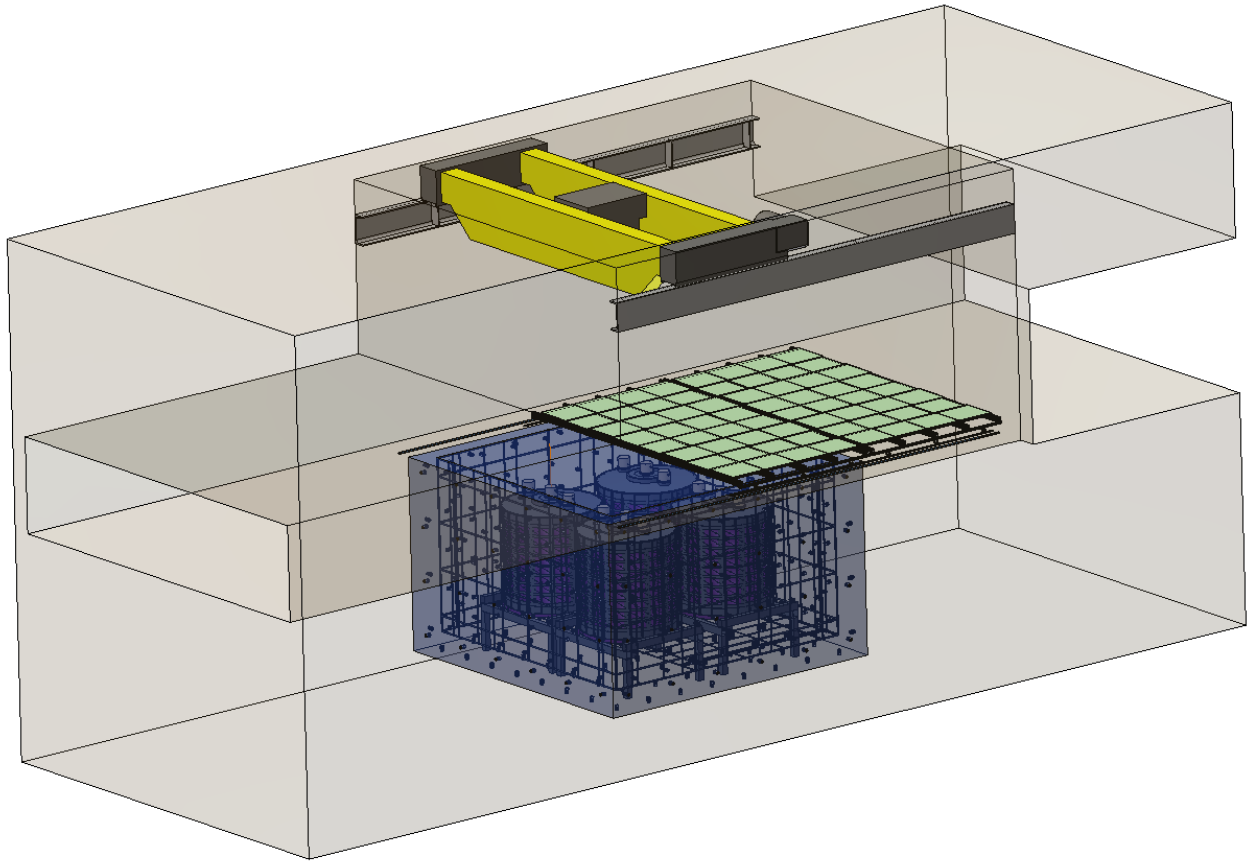


Fig. 1.14. Layout of the baseline design of the Daya Bay detector at the far site. Four antineutrino detector modules are shielded by a 1.5 m-thick active water Cherenkov shield. Surrounding this shield and optically isolated from it is another 1-meter of water Cherenkov shield. The muon system is completed with RPCs at the top.

- Employ three-zone detector modules partitioned with two acrylic tanks as shown in Fig. 1.15. The target volume is defined by the physical dimensions of the central region of Gd-LS. This target volume is surrounded by an intermediate region filled with normal LS to catch γ rays escaping from the central region. The LS regions are embedded in a volume of mineral oil to separate the PMTs from the LS and suppress natural radioactivity from the PMT glass and other external sources.

Four of these modules, each with 20 ton target mass, will be deployed at the far site to obtain sufficient statistics and two modules will be deployed at each near site, enabling cross calibrations. Deploying an equal number of near and far detectors allows for flexibility in analyzing the data to minimize the

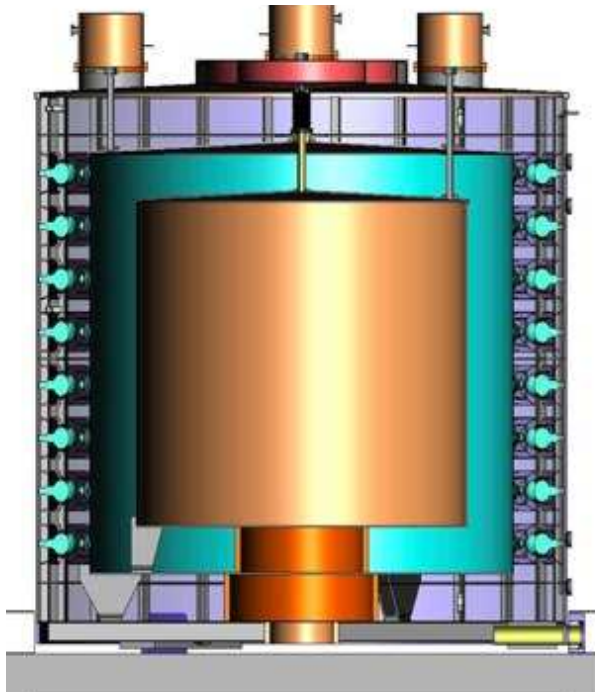


Fig. 1.15. Cross sectional slice of a 3-zone antineutrino detector module showing the inner acrylic vessel holding the Gd-LS at the center (20 ton), LS between the acrylic vessels (20 ton) and mineral oil (40 ton) in the outer region. The PMTs are mounted on the inner surface of the stainless steel tank.

systematic uncertainties, such as analyzing with matched near-far pairs.

In this design, the homogeneous target volume is well determined without a position cut since antineutrinos interacted in the unloaded LS will not in general satisfy the high neutron-capture energy requirement with Gd. Each vessel will be carefully measured to determine its volume and each vessel will be filled with the same set of mass-flow and volumetric flow meters to minimize any variation in the relative detector volume and mass. The effect of neutron spill-in and spill-out across the boundary between the two LS regions will be cancelled when pairs of identical detector modules are used at the near and far sites. With the shielding of mineral oil, the singles rate will be reduced substantially. The trigger threshold can thus be lowered to below 1.0 MeV, providing $\sim 100\%$ detection efficiency for the prompt positron signal.

- The Gd-LS, which is the antineutrino target, should have the same composition and fraction of hydrogen for each pair of detectors (one at a near site and the other at the far site). The detectors will be filled from a common storage vessel to assure that the composition of the LS is the same. Other detector components such as unloaded LS and PMTs will be characterized and distributed evenly to a pair of detector modules during assembly to equalize the properties of the modules.
- The energy resolution should be better than 15% at 1 MeV. Good energy resolution is desirable for reducing the energy-related systematic uncertainty on the neutron energy cut. Good energy resolution is also important for studying spectral distortion as a signature of neutrino oscillation. The primary driver for the energy resolution is to achieve sufficient energy calibration precision for neutron captures throughout the detector volume in a reasonable time.

- The time resolution should be better than 1 ns for determining the event time and for studying backgrounds.

Detector modules of different shapes, including cubical, cylindrical, and spherical, have been considered. From the point of view of ease of construction cubical and cylindrical shapes are particularly attractive. Monte Carlo simulation shows that cylindrical modules can provide better energy and position resolutions for the same number of PMTs. Figure 1.15 shows the structure of a cylindrical module. The PMTs are arranged along the circumference of the outer cylinder. The surfaces at the top and the bottom of the outermost acrylic cylinder are covered with a diffuse reflective material. Such an arrangement is feasible since 1) the event vertex is determined only with the center of gravity of the charge, not relying on the time-of-flight information,^{||} 2) the fiducial volume is well defined with a three-zone structure, thus no accurate vertex information is required. Details of the antineutrino detector will be discussed in Chapter ??.

1.3.2.2 Muon detector

Since most backgrounds originate from cosmic-ray muon interactions with nearby materials, it is desirable to have a very efficient muon detector with some tracking capability. This enables the study and rejection of cosmogenic backgrounds. The two selected detector technologies are water Cherenkov counters and RPCs. The combined water Cherenkov detector and RPC can achieve muon detection efficiencies close to 100%. Furthermore, these two independent detectors can cross check each other. Their inefficiencies and the associated uncertainties can be well determined by cross calibration during data taking. We expect the inefficiency will be smaller than 0.5% and the uncertainty of the inefficiency will be better than 0.25%.

Besides being a shield against ambient radiation, the water shield can also be utilized as a water Cherenkov counter by installing PMTs in the water. The water Cherenkov detector is based on proven technology, and known to be very reliable. With sufficient PMT coverage and reflective surfaces, the efficiency of detecting muons should exceed 95%. The current baseline design of the water shield is a water pool, similar to a swimming pool with a dimensions of 16 m (length) \times 16 m (width) \times 10 m (height) for the far hall containing four detector modules, as shown in Fig. 1.14. The PMTs of the water Cherenkov counters are mounted facing the inside of the water volume. This is a simple and proven technology with very limited safety concerns. The water will effectively shield the antineutrino detectors from radioactivity in the surrounding rocks and from radon, with the attractive features of being simple, cost-effective and rapidly deployable.

RPCs are very economical for instrumenting large area, and simple to fabricate. The Bakelite-based RPC developed by IHEP for the BES-III detector has a typical efficiency of 95% and noise rate of 0.1 Hz/cm² per layer [31]. A possible configuration is to build four layers of RPC, and require three out of four layers to have a hit within a time window of 20 ns to define a muon event. Such a scheme has high efficiency and low noise rate. Although RPCs provide an ideal large-area muon detector due to their light weight, good performance, excellent position resolution and low cost, it is hard to put them in water to fully surround the water pool. The best choice is to use them only on the top of the water pool.

1.3.2.3 WBS

The plan for construction of the Daya Bay detector is described by the Daya Bay work breakdown structure (WBS), which has nine major categories as shown in Table 1.3.

REFERENCES

1. B. T. Cleveland *et al.*, *Astrophys. J.* **496** (1998) 505.

^{||}Although time information may not be used in reconstructing the event vertex, it will be used in background studies. A time resolution of 0.5 ns can be easily realized in the readout electronics.

WBS element	Task Name
1.1	Antineutrino Detector
1.2	Muon System
1.3	Calibration and Monitoring Systems
1.4	Electronics, Trigger, DAQ and Online
1.5	Offline
1.6	Conventional Construction and Equipment
1.7	Installation and Test
1.8	Integration
1.9	Project Management

Table 1.3. Daya Bay Work Breakdown Structure (WBS) shown at L2.

2. Y. Fukuda *et al.* (SuperK Collaboration), Phys. Rev. Lett., **81** (1998) 1158 [arXiv:hep-ex/9805021]; **82** (1999) 2430 [arXiv:hep-ex/9812011]; S. Fukuda *et al.*, Phys. Rev. Lett. **86** (2001) 5651 [arXiv:hep-ex/010302]; M. B. Smy *et al.*, Phys. Rev. **D69** (2004) 011104 [arXiv:hep-ex/0309011].
3. J. N. Abdurashitov *et al.* (SAGE Collaboration), J. Exp. Theor. Phys. **95** (2002) 181 [arXiv:astro-ph/0204245]; W. Hampel *et al.* (GALLEX Collaboration), Phys. Lett. **B447** (1999) 127; M. Altman *et al.* (GNO Collaboration), Phys. Lett. **B490** (2000) 16 [arXiv:hep-ex/0006034].
4. Q.R. Ahmad *et al.* (SNO Collaboration), Phys. Rev. Lett **87** 071301 [arXiv:nucl-ex/0106015]; **89** (2002) 011301 [arXiv:nucl-ex/0204008]; **89** (2002) 011302 [arXiv:nucl-ex/0204009]; **92** (2004) 181301 [arXiv:nucl-ex/0309004]; Phys. Rev. **C72** (2005) 055502 [arXiv:nucl-ex/0502021].
5. Y. Fukuda *et al.* (SuperK Collaboration), Phys. Lett. **B433** (1998) 9 [arXiv:hep-ex/9803006]; **B436** (1998) 33 [arXiv:hep-ex/9805006]; Phys. Rev. Lett., **81** (1998) 1562 [arXiv:hep-ex/9807003]; S. Fukuda *et al.*, Phys. Rev. Lett. **85** (2000) 3999 [arXiv:hep-ex/0009001]; Y. Ashie *et al.*, Phys. Rev. Lett. **93** (2004) 101801 [arXiv:hep-ex/0404034].
6. K. Eguchi *et al.* (KamLAND Collaboration), Phys. Rev. Lett., **90** (2003) 021802 [arXiv:hep-ex/0212021]; **94** (2005) 081801 [arXiv:hep-ex/0406035].
7. E. Aliu *et al.* (K2K Collaboration), Phys. Rev. Lett. **94** (2005) 081802 [arXiv:hep-ex/0411038].
8. D.G. Michael *et al.* (MINOS Collaboration), Phys. Rev. Lett. **97** (2006) 191801 [arXiv:hep-ex/0607088].
9. Z. Maki, M. Nakagawa, and S. Sakata, Prog. Theor. Phys. **28** (1962) 870; B. Pontecorvo, Sov. Phys. JETP **26** (1968) 984; V.N. Gribov and B. Pontecorvo, Phys. Lett. **28B** (1969) 493.
10. G.L. Fogli, E. Lisi, A. Marrone, and A. Palazzo, and A.M. Rotunno, 40th Rencontres de Moriond on Electroweak Interactions and Unified Theories, La Thuile, Aosta Valley, Italy, 5-12 March 2005 [arXiv:hep-ph/0506307].
11. T. Schwetz, Talk given at 2nd Scandinavian Neutrino Workshop (SNOW 2006, Stockholm Sweden, 2-6 May 2006 [arXiv:hep-ph/0606060].
12. M. Apollonio *et al.* (Chooz Collaboration), Eur. Phys. J. **C27**, 331 (2003) [arXiv:hep-ex/0301017].
13. K. Anderson, *et al.*, *White paper report on using nuclear reactors to search for a value of θ_{13}* , arXiv:hep-ex/0402041.
14. 'Recommendations to the Department of Energy and the National Science Foundation on a U.S. Program of Reactor- and Accelerator-based Neutrino Oscillations Experiments', <http://www.science.doe.gov/hep/NuSAG2ndRptFeb2006.pdf>
15. *The Neutrino Matrix*, <http://www.aps.org/neutrino/>
16. M.F. James, J. Nucl. Energy **23** 517 (1969).
17. L. Miller, Ph.D Thesis, Stanford University, 2000, unpublished.
18. V.I. Kopeikin, Phys. Atom. Nucl. **66** (2003) 472 [arXiv:hep-ph/0110030].
19. B. Achkar *et al.*, Phys. Lett. **B374** 243 (1996).

20. K. Schreckenbach *et al.*, Phys. Lett. **B160**, 325 (1985); A. A. Hahn *et al.*, Phys. Lett. **B218**, 365 (1989).
21. P. Vogel and J. Engel, Phys. Rev. **D39**, 3378 (1989).
22. P. Vogel and J. F. Beacom, Phys. Rev. **D60**, 053003 (1999) [arXiv:hep-ph/9903554].
23. L.A. Mikaelyan and V.V. Sinev, Phys. Atomic Nucl. **63** 1002 (2000) [arXiv:hep-ex/9908047].
24. M. Kuze *et al.*, *The KASKA project - a Japanese medium-baseline reactor-neutrino oscillation experiment to measure the mixing angle θ_{13}* , arXiv:hep-ex/9908047.
25. K.K.Joo, *Progress Report on RENO*, talk presented at NOW 2006, Otranto, Italy, September 9-16, 2006.
26. F. Ardellier *et al.* (Double Chooz Collaboration), *Double Chooz: A Search for the Neutrino Mixing Angle θ_{13}* , arXiv:hep-ex/0606025.
27. L.A. Mikaelyan and V. V. Sinev, Phys. Atom. Nucl. **63**, 1002 (2000); L. Mikaelyan, Nucl. Phys. Proc. Suppl. **91**, 120 (2001); L.A. Mikaelyan, Phys. Atom. Nucl. **65**, 1173 (2002).
28. *Report of Preliminary Feasibility Study of Site Selection for the Daya Bay Neutrino Experiment*, prepared by Beijing Institute of Nuclear Energy, September, 2004.
29. M. Apollonio *et al.* (Chooz Collaboration), Phys. Lett. **B420**, 397 (1998); Phys. Lett. **B466**, 415 (1999); Eur. Phys. J. **C27**, 331 (2003).
30. F. Boehm *et al.* (Palo Verde Collaboration), Phys. Rev. Lett. **84**, 3764 (2000) [arXiv:hep-ex/9912050]; Phys. Rev. **D62**, 072002 (2000) [arXiv:hep-ex/0003022]; Phys. Rev. **D64**, 112001 (2001) [arXiv:hep-ex/0107009]; A. Piepke *et al.*, Nucl. Instr. and Meth. **A432**, 392 (1999).
31. J.W. Zhang *et al.*, High Energy Phys. and Nucl. Phys., **27**, 615 (2003); JiaWen Zhang *et al.*, Nucl. Inst. Meth. **A540**, 102 (2005).